Ca^{2+} entry through mechanotransduction channels localizes BAIAP2L2 to stereocilia tips

Julia Halford, Michael Bateschell, and Peter G. Barr-Gillespie*
Oregon Hearing Research Center & Vollum Institute, Oregon Health & Science University, Portland, OR 97239

ABSTRACT **Brain-specific angiogenesis inhibitor 1-associated protein 2-like protein 2 (BAIAP2L2), a membrane-binding protein required for the maintenance of mechanotransduction in hair cells, is selectively retained at the tips of transducing stereocilia. BAIAP2L2 trafficked to stereocilia tips in the absence of EPS8, but EPS8 increased the efficiency of localization. A tripartite complex of BAIAP2L2, EPS8, and MYO15A formed efficiently in vitro, and these three proteins robustly targeted to filopodia tips when coexpressed in cultured cells. Mice lacking functional transduction channels no longer concentrated BAIAP2L2 at row 2 stereocilia tips, a result that was phenocopied by blocking channels with tubocurarine in cochlear explants. Transduction channels permit Ca^{2+} entry into stereocilia, and we found that membrane localization of BAIAP2L2 was enhanced in the presence of Ca^{2+}. Finally, reduction of intracellular Ca^{2+} in hair cells using BAPTA-AM led to a loss of BAIAP2L2 at stereocilia tips. Taken together, our results show that a MYO15A-EPS8 complex transports BAIAP2L2 to stereocilia tips, and Ca^{2+} entry through open channels at row 2 tips retains BAIAP2L2 there.**

Monitoring Editor
Alpha Yap
University of Queensland

Received: Oct 15, 2021
Revised: Dec 20, 2021
Accepted: Jan 10, 2022

INTRODUCTION

Vertebrate hearing relies on the transduction of the mechanical stimulus of sound into an electrical signal. Hair bundles, which project from the apical surface of sensory hair cells, mediate this process (Hudspeth, 1997). Bundles consist of ~100 stereocilia, membrane-enveloped protrusions of filamentous actin, organized into distinct rows that form a staircase pattern (Tilney *et al.*, 1980; Kaltenbach *et al.*, 1994). In mammalian auditory hair cells, the staircase includes the tall and thick row 1, the shorter and thick row 2, and the shortest and thinnest row 3. Transduction channels, located at the tips of rows 2 and 3 stereocilia (Beurg *et al.*, 2009), are partially open at rest but open even further as a stimulus deflects the bundle toward the tallest row. Tip links, which are extracellular protein filaments that extend from the tip of a transducing stereocilium to the shaft of its nearest tall neighbor, convey stimulus force to transduction channels (Fettiplace and Kim, 2014).

Transduction modulates the dimensions of stereocilia in the hair bundle. Mouse mutants lacking components of the transduction apparatus have altered stereocilia organization and dimensions (Cosgrove and Zallocchi, 2014). Further, blocking transduction channels or breaking tip links induces reversible changes in stereocilia length within 1–2 d (Velez-Ortega *et al.*, 2017; Krey *et al.*, 2020). Disruption of transduction also affects distribution of key bundle proteins (Krey *et al.*, 2020; McGrath *et al.*, 2021). Finally, Ca^{2+} entry through transduction channels regulates the function of many stereocilia proteins (Fettiplace, 2017).

We and others showed previously that brain-specific angiogenesis inhibitor 1-associated protein 2-like protein 2 (BAIAP2L2) stabilizes the shorter transducing stereocilia. BAIAP2L2 enriches at the tips of those stereocilia, interacts with the actin regulator EPS8, and depends on MYO15A for localization (Carlton *et al.*, 2021; Yan *et al.*, 2021). These results suggested that BAIAP2L2 may be transported by the transduction-regulated MYO15A-EPS8 complex (Ebrahim *et al.*, 2016; Manor *et al.*, 2011; Lin *et al.*, 2021), which carries other hair-bundle proteins (Tadenev *et al.*, 2019; Krey *et al.*, 2020).

This article was published online ahead of print in MBoC in Press (http://www.molbiolcell.org/cgi/doi/10.1091/mbc.E21-10-0491) on January 19, 2022.

Source data: Contains uncropped and unprocessed images with annotations for blots displayed in Figures 2I, 2J and S2F, S2G.

Author contributions: conceptualization, P.G.B-G. and J.H.; data curation, J.H.; formal analysis, J.H.; funding acquisition, P.G.B-G.; investigation, J.H. and M.B.; methodology, all authors; project administration, P.G.B-G.; resources, P.G.B-G. and M.B.; software, n/a; supervision, P.G.B-G.; validation, J.H. (*Eps8*$^{\Delta 818}$ loss of immunoreactivity) and M.B. (*Eps8*$^{\Delta 818}$ sequencing); visualization, J.H. and P.G.B-G.; writing (original draft), J.H. and P.G.B-G.; writing (review and editing), all authors.

*Address correspondence to: Peter G. Barr-Gillespie (gillespp@ohsu.edu).

Abbreviations used: BAIAP2L2, brain-specific angiogenesis inhibitor 1-associated protein 2-like protein 2; DIV, days in vitro; gDNA, guide RNA; HMM, heavy meromyosin; IHC, inner hair cell; iono, ionomycin; IQR, interquartile range; PLA, proximity ligation assay; RFP, red fluorescent protein; RNP, ribonucleoprotein; ROI, region of interest.

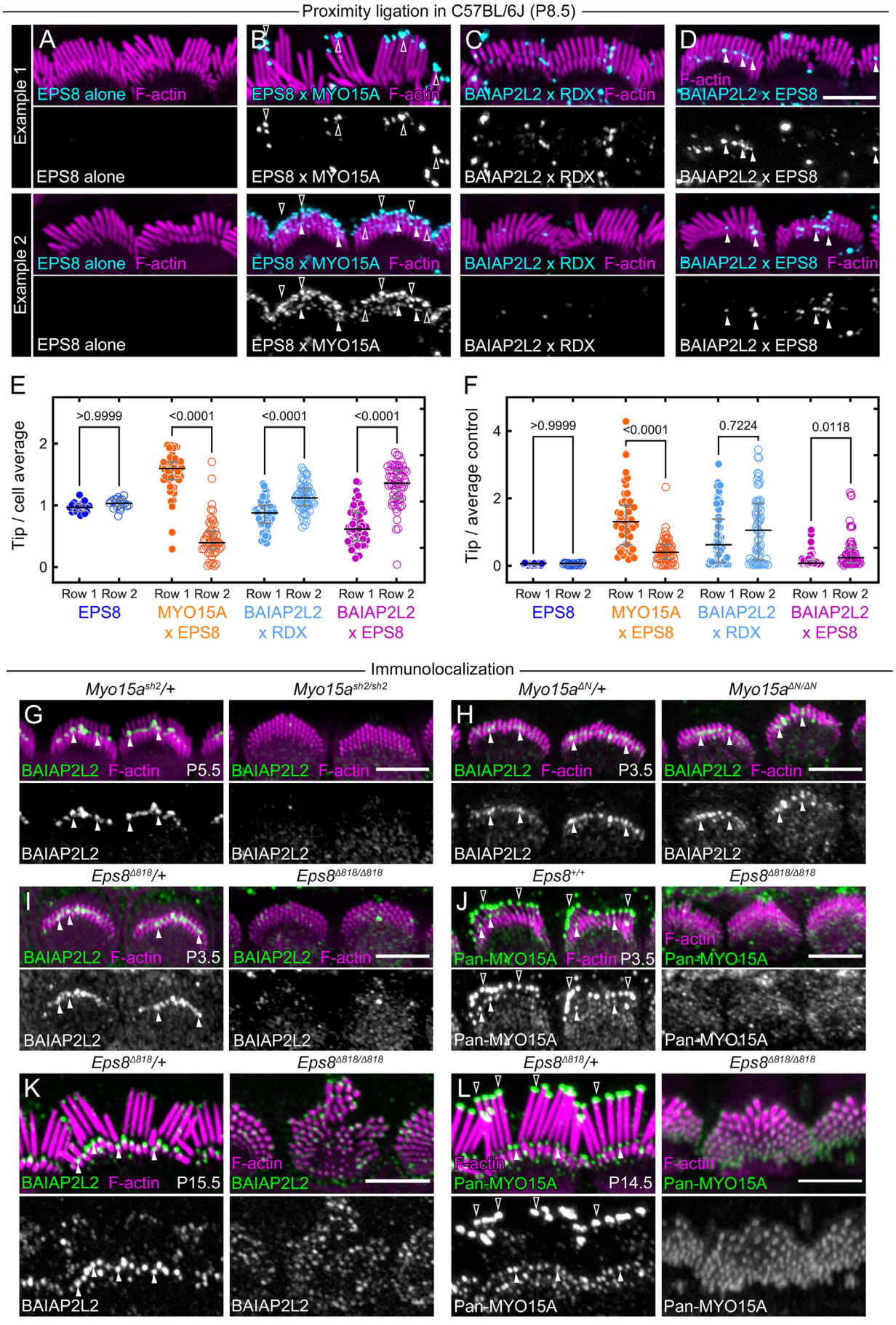
Proximity ligation in C57BL/6J (P8.5)
Example 1
Example 2
A
EPS8 alone F-actin
EPS8 alone
B
EPS8 x MYO15A F-actin
EPS8 x MYO15A
C
BAIAP2L2 x RDX F-actin
BAIAP2L2 x RDX
D
F-actin
BAIAP2L2 x EPS8
BAIAP2L2 x EPS8
E
Tip / cell average
>0.9999
<0.0001
<0.0001
<0.0001
Row 1 Row 2
EPS8
MYO15A x EPS8
BAIAP2L2 x RDX
BAIAP2L2 x EPS8
F
Tip / average control
>0.9999
<0.0001
0.7224
0.0118
Immunolocalization
Myo15a^sh2/+
Myo15a^sh2/sh2
Myo15a^ΔN/+
Myo15a^ΔN/ΔN
G
BAIAP2L2 F-actin P5.5
BAIAP2L2
H
BAIAP2L2 F-actin P3.5
BAIAP2L2
Eps8^Δ818/+
Eps8^Δ818/Δ818
Eps8^+/+
I
BAIAP2L2 F-actin P3.5
BAIAP2L2
J
Pan-MYO15A F-actin P3.5
F-actin
Pan-MYO15A
Pan-MYO15A
K
BAIAP2L2 F-actin P15.5
F-actin
BAIAP2L2
L
F-actin
Pan-MYO15A P14.5
F-actin
Pan-MYO15A

MYO15A and EPS8 are both essential for normal bundle development; mutants in either gene produce bundles with short, narrow stereocilia (Belyantseva *et al.*, 2003; Zampini *et al.*, 2011). BAIAP2L2 also can bind EPS8L2 and CAPZB, which both concentrate at row 2 tips, unlike EPS8 and MYO15A (Yan *et al.*, 2021).

BAIAP2L2 is an inverse Bin/amphiphysin/Rvs (I-BAR) domain protein (Pykalainen *et al.*, 2011; Zhao *et al.*, 2011), a family that links the plasma membrane to the actin cytoskeleton. The I-BAR domain of BAIAP2L2 binds phosphoinositide-containing membranes (Pykalainen *et al.*, 2011), and $PI(4,5)P_2$ is enriched at stereocilia tips (Hirono *et al.*, 2004; Effertz *et al.*, 2017). Moreover, Ca^{2+} modulates protein interactions with phosphoinositides (Bilkova *et al.*, 2017), so Ca^{2+} influx into stereocilia suggests that transduction could modulate BAIAP2L2's association with the stereocilia tip membrane.

Here we show that the MYO15A-EPS8 complex optimally transports BAIAP2L2 within actin-based projections, and that transduction concentrates BAIAP2L2 at stereocilia tips. We also show that BAIAP2L2 association with the plasma membrane is enhanced when Ca^{2+} is elevated, and that chelation of intracellular Ca^{2+} interferes with BAIAP2L2 localization at stereocilia tips. We therefore suggest that BAIAP2L2 delivered to stereocilia tips by MYO15A-EPS8 complexes is subsequently retained there only if Ca^{2+} entering through open transduction channels produces an environment that favors BAIAP2L2 membrane binding.

RESULTS AND DISCUSSION

BAIAP2L2 targeting in stereocilia requires MYO15A but not EPS8

Because BAIAP2L2 localizes abnormally in null mutants of *Myo15a* and *Eps8* (Carlton *et al.*, 2021), we tested for the presence of a BAIAP2L2-EPS8 complex in inner hair cells (IHCs) from C57BL/6J mice using a proximity ligation assay (PLA), an antibody-based method for assessing the physical juxtaposition of molecules in situ (Soderberg *et al.*, 2006) (Figure 1, A–D). As a negative control, minimal signal was observed when PLA was carried out for EPS8 alone (Figure 1A). As a positive control, PLA for MYO15A and EPS8 produced strong labeling at row 1 stereocilia tips as well as lower levels of labeling at row 2 tips (Figure 1B); this distribution was expected given their known locations (Manor *et al.*, 2011; Lin *et al.*, 2021). PLA for the combination of BAIAP2L2 and EPS8 produced discrete labeling at row 2 stereocilia tips (Figure 1D) despite the higher concentration of EPS8 at row 1 stereocilia tips compared with those of row 2. We also examined PLA between BAIAP2L2 and RDX, which is present along stereocilia membranes (Kitajiri *et al.*, 2004). PLA with antibodies for BAIAP2L2 and RDX (Figure 1C), which we have previously shown do not interact (Carlton *et al.*, 2021), produced labeling with less marked preference toward either row of stereocilia.

We quantified the PLA signal in these experiments using two different normalization methods; BAIAP2L2-EPS8 PLA signal for row 2 was higher than for row 1 when signal was normalized within a cell (Figure 1E; $p < 0.0001$) or across all PLA experiments (Figure 1F; $p = 0.012$). The former method emphasizes relative differences within a cell, while the latter method also reflects the amplitude of the PLA signal. Although PLA data showed considerable variability (Figure 1, A–F; Supplemental Figure S1, A–C), the results suggested that a BAIAP2L2-EPS8 complex forms in hair cells.

We examined the contributions to BAIAP2L2 trafficking by the short and long MYO15A splice isoforms (Fang *et al.*, 2015; Rehman *et al.*, 2016). We first confirmed that BAIAP2L2 was not detected at the stereocilia tips at P5.5 in *Myo15a*$^{sh2/sh2}$ mice (Figure 1G) which lack functional MYO15A. We then examined P5 cochleas from *Myo15a*$^{\Delta N}$ mice which specifically lack MYO15A-1 (Fang *et al.*, 2015). BAIAP2L2 localized to tips of transducing stereocilia in *Myo15a*$^{\Delta N/\Delta N}$ hair bundles, showing that MYO15A-1 is not required for tip targeting; normal targeting must instead require MYO15A-2 or MYO15A-3 (Figure 1H).

To examine the role of EPS8 in BAIAP2L2 targeting, we used i-GONAD (Gurumurthy *et al.*, 2019; Ohtsuka and Sato, 2019) to generate *Eps8*$^{\Delta 818}$, a new *Eps8* mutant allele (Supplemental Figure S1D). Targeting two separate gRNAs to exons 3 and 5, we obtained several G0 pups containing indels. The founder for the selected line, Δ818, contained a large deletion spanning 10,818 base pairs of genomic DNA between exons 3 and 5 (115,524–126,324). EPS8 immunoreactivity was absent in *Eps8*$^{\Delta 818/\Delta 818}$ hair cells (Supplemental Figure S1E).

In *Eps8*$^{\Delta 818/\Delta 818}$ mice, we unexpectedly detected BAIAP2L2 signal at the tips of all stereocilia; tip signal was more apparent at P15.5 than P3.5 (Figure 1, I and K). As we had previously suggested that BAIAP2L2 was absent from all stereocilia in mice lacking *Eps8* (Carlton *et al.*, 2021), we tested the antibody used previously (Atlas Cat# HPA003043) and found that anti-BAIAP2L2 signal was still present in our *Eps8* knockout, albeit reduced compared with heterozygote littermates (Supplemental Figure S1F). These results suggested that MYO15A might traffic BAIAP2L2 without EPS8. Indeed, we found that MYO15A was present at all stereocilia tips in *Eps8*$^{\Delta 818/\Delta 818}$ at both P3.5 and P14.5 (Figure 1, J and L).

EPS8 enhances MYO15A-BAIAP2L2 trafficking

To test if BAIAP2L2 could interact directly or indirectly with MYO15A without EPS8, we used nanoscale pull down (NanoSPD) in HeLa cells to examine the interaction (Bird *et al.*, 2017). In NanoSPD, a filopodia-targeting GFP-MYO10-bait and a red fluorescent protein (RFP)-tagged prey protein are coexpressed; if they interact, the GFP-MYO10-bait concentrates the RFP-prey at filopodial tips. *mCherry-Baiap2l2* was cotransfected with either the negative

FIGURE 1: BAIAP2L2 localizes with EPS8 but does not require it for targeting. (A-D) PLA in P8.5 C57BL/6J IHCs. (A) Single primary antibody (anti-EPS8). (B) Anti-MYO15A and anti-EPS8. (C) Anti-RDX and anti-BAIAP2L2. (D) Anti-BAIAP2L2 and anti-EPS8. Examples from two separate experiments are included to show range of signal. (E, F) Quantification of PLA signal, normalized by cell (E), or normalized by MYO15A-EPS8 signal per experiment (F). Data plotted with median and interquartile range (IQR); individual points are average stereocilia tip signal at row 1 or row 2 per cell. Data were analyzed by Kruskal–Wallis tests, followed by Dunn's multiple comparisons; *P* values are indicated in the plot (Supplemental Table S1 for details). (G–I, K) Anti-BAIAP2L2 signal in heterozygote and knockout IHCs. (G) *Myo15a*^{sh2}/+, *Myo15a*$^{sh2/sh2}$; P5.5. (H) *Myo15a*$^{\Delta N}$/+, *Myo15a*$^{\Delta N/\Delta N}$; P5. (I) *Eps8*$^{\Delta 818}$/+, *Eps8*$^{\Delta 818/\Delta 818}$; P3.5. (K) *Eps8*$^{\Delta 818}$/+, *Eps8*$^{\Delta 818/\Delta 818}$; P15.5. (J) Anti-MYO15A signal in *Eps8*$^{+/+}$, *Eps8* $^{\Delta 818/\Delta 818}$; P3.5. (L) Anti-MYO15A signal in *Eps8*$^{\Delta 818}$/+, *Eps8*$^{\Delta 818/\Delta 818}$; P14.5. Antibody signal intensity was matched between heterozygote and knockout pairs in each panel but was not comparable across ages or across mutants. Empty arrowheads at row 1 tips, solid arrowheads at row 2 tips. Scale, 5 μm.

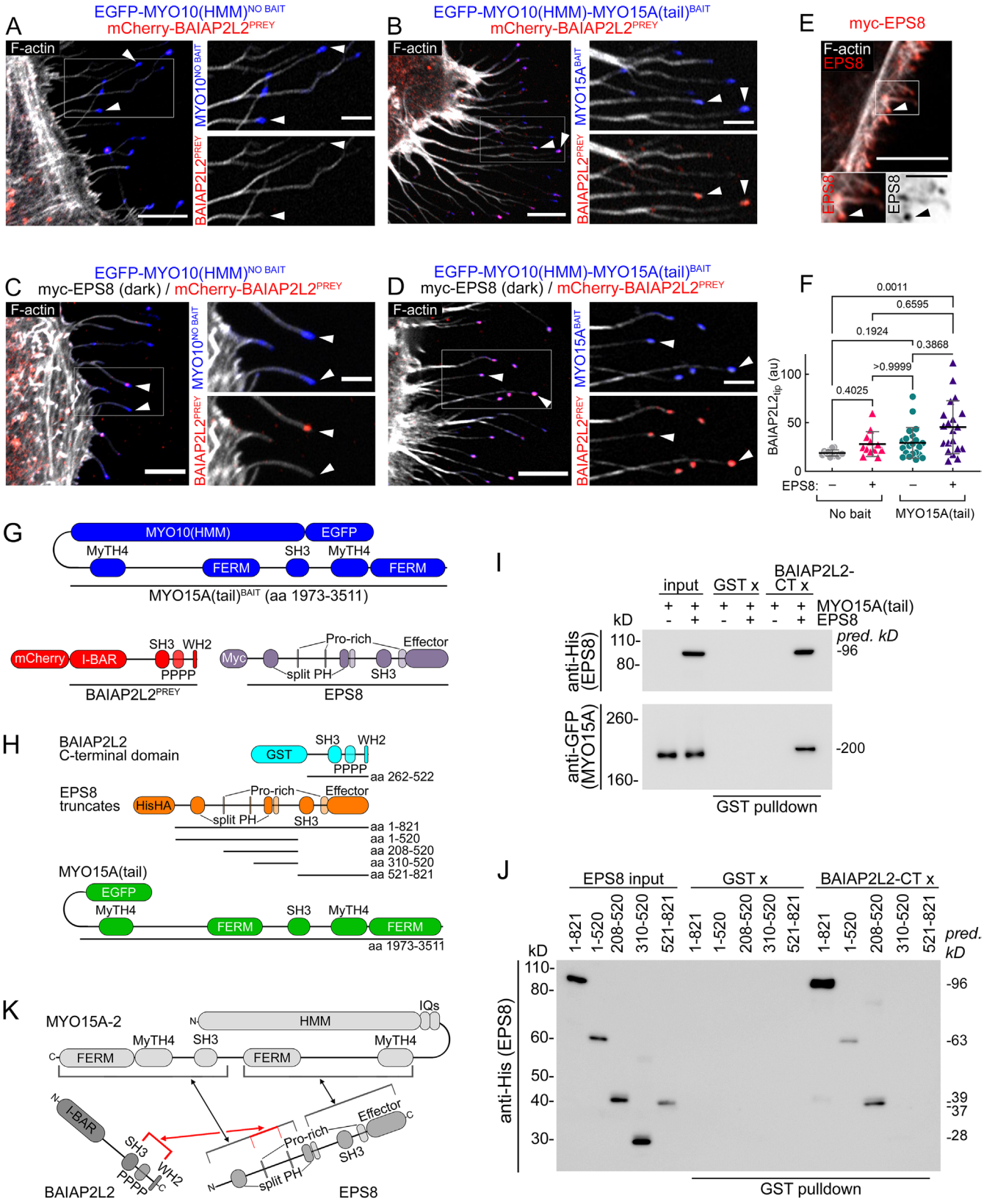

FIGURE 2: MYO15A, EPS8, and BAIAP2L2 form a tripartite complex. (A–G) NanoSPD in HeLa cells. (A, B) mCherry-BAIAP2L2^{PREY} coexpressed with (A) EGFP-MYO10$^{NO\text{-}BAIT}$ or (B) EGFP-MYO10-MYO15A(tail)^{BAIT}. (C, D) Myc-EPS8 and mCherry-BAIAP2L2^{PREY} coexpressed with (C) EGFP-MYO10$^{NO\text{-}BAIT}$ or (D) EGFP-MYO10-MYO15A(tail)^{BAIT}. Myc-EPS8 and mCherry-BAIAP2L2 were expressed using a P2A-linked bicistronic plasmid. (E) myc-EPS8 expressed alone. Scale, 5 μm in micrographs on the left side of each panel or 2 μm in enlarged insets. (F) Quantitation of BAIAP2L2^{PREY} fluorescence at filopodial tips for conditions shown in A–D. Data plotted with median and IQR; individual points are average

control *gfp-Myo10* heavy meromyosin (HMM) or *gfp-Myo10*(HMM)-*Myo15a*(tail); the MYO15A(tail) sequence is shared by all MYO15A splice forms. mCherry-BAIAP2L2 signal at filopodial tips was then quantified. BAIAP2L2 did not target to filopodia tips when expressed with MYO10(HMM) (Figure 2A and Supplemental Figure S2A) but was often localized at filopodial tips when coexpressed with MYO10(HMM)-MYO15A(tail) (Figure 2B; Supplemental Figure S2, B and E). Variability in the NanoSPD results meant that filopodial tip enrichment of BAIAP2L2 in the presence of MYO15A was not significant (Figure 2F; Supplemental Table S1).

EPS8 influences the putative interaction between BAIAP2L2 and MYO15A. We cotransfected *myc-Eps8/P2A/mCherry-Baiap2l2* with either *gfp-Myo10*(HMM)-*Myo15a*(tail) or *gfp-Myo10*(HMM) (Figure 2, C and D; Supplemental Figure S2, C and D) and found that BAIAP2L2 targeting to filopodia tips increased with the addition of EPS8. In the absence of MYO15A(tail) and the presence of EPS8 (Figure 2C; Supplemental Figure S2, C and E), BAIAP2L2 was found at filopodia tips at similar levels as BAIAP2L2 coexpressed with MYO15A(tail) (Figure 2F; Supplemental Table S1). This result indicates that EPS8 does not require MYO15A(tail) to target to filopodia tips and is consistent with other observations indicating that EPS8 localizes at the tips of filopodia and microvilli (Figure 2E) (Menna *et al.*, 2009; Postema *et al.*, 2018). In the hair bundle, however, EPS8 requires MYO15A to localize to stereocilia tips (Manor *et al.*, 2011). Elevated BAIAP2L2 at filopodia tips with coexpression of EPS8 was also consistent with our previous data demonstrating an interaction between BAIAP2L2 and EPS8.

In the presence of both MYO15A(tail) and EPS8 (Figure 2D), BAIAP2L2 was most frequently found at filopodia tips and was at significantly higher levels than in BAIAP2L2/no-bait (Figure 2F; Supplemental Figure S2E; Supplemental Table S1). BAIAP2L2 transport thus was enhanced by the combined presence of MYO15A and EPS8.

We used in vitro pull-down experiments to determine whether EPS8 and MYO15A traffic BAIAP2L2 in a tripartite complex. While MYO15A(tail) did not bind directly to the C-terminal domain of BAIAP2L2, inclusion of full-length EPS8 enabled the coprecipitation of MYO15A(tail) with the C-terminal domain of BAIAP2L2 (Figure 2I).

As EPS8 can bind either the N-terminal (Manor *et al.*, 2011) or the C-terminal (Lin *et al.*, 2021) MyTH-FERM domains of MYO15A(tail), we sought to determine the BAIAP2L2 binding region within EPS8. Testing the C-terminal domain of BAIAP2L2 against a series of EPS8 truncates using an in vitro pull-down assay (Figure 2, H and J), we found that the BAIAP2L2 binding region maps to residues 208–310 of EPS8, which includes proline-rich motifs. The full-length EPS8 protein produced the strongest pull-down signal (Figure 2J), however, suggesting that other domains may contribute as well.

Our results demonstrate the formation of a tripartite complex of MYO15A, EPS8, and BAIAP2L2 (Figure 2K) and suggest that this complex transports BAIAP2L2 in hair bundles. Although the appearance of BAIAP2L2 at all stereocilia tips in *Eps8*-null bundles suggested that it could be trafficked without EPS8, PLA experiments indicated that EPS8 and BAIAP2L2 were localized in close proximity in wild-type row 2 stereocilia. Moreover, EPS8 significantly increased the efficiency of BAIAP2L2 filopodial-tip trafficking in HeLa cells, especially in the presence of MYO15A. By in vitro pull down, BAIAP2L2 and MYO15A were unable to interact directly with each other; while MYO15A might transport BAIAP2L2 in the absence of EPS8, the MYO15A-EPS8 complex transports BAIAP2L2 more efficiently.

Transduction mutants fail to enrich BAIAP2L2

Selective localization of BAIAP2L2 to tips of transducing stereocilia suggested that transduction itself might influence targeting. To test this hypothesis, we examined IHCs from mice lacking different components of the transduction apparatus and localized BAIAP2L2 by immunocytochemistry. We examined mutant mouse lines lacking either both *Tmc* genes (Figure 3, A and B) or *Tmie* (Figure 3, C and D), lines that presumably lack the channel pore (Zhao *et al.*, 2014; Kawashima *et al.*, 2015; Pan *et al.*, 2018). We also tested *Pcdh15*^{av3} mice (Figure 3, E and F) which lack tip links (Ahmed *et al.*, 2006). We localized BAIAP2L2 in cochleas at P8.5, when hair bundles are still developing, and at P21.5, when bundles are effectively mature (Krey *et al.*, 2020).

As seen previously, BAIAP2L2 localized in heterozygote control IHCs to row 2 and 3 tips; at P8.5, BAIAP2L2 labeling was most apparent at row 2 stereocilia tips, while at P21.5, labeling extended below stereocilia tips and became more evident at row 3 tips as well (Figure 3D). In contrast, BAIAP2L2 was absent from all stereocilia tips at both time points in transduction mutants regardless of which component of the transduction apparatus was absent. Rather than redistributing like other stereocilia proteins (Krey *et al.*, 2020), residual BAIAP2L2 labeling was sparse and no longer row restricted (Figure 3D). BAIAP2L2 localization thus may rely on the active transduction conductance to localize to stereocilia tips.

Maintenance of BAIAP2L2 at stereocilia tips depends on open transduction channels

To confirm that active transduction localizes BAIAP2L2, we tested whether a transduction block in cultured cochlear explants from C57BL/6J mice led to redistribution of stereocilia BAIAP2L2 in IHCs. After treatment of P4.5 cochleas for 2 d in vitro (DIV) with 100 µM tubocurarine, which effectively blocks transduction currents (Glowatzki *et al.*, 1997; Krey *et al.*, 2020), BAIAP2L2 was no longer detectable in hair bundles (Figure 4, A and B; Supplemental Table S1). By contrast, tubocurarine treatment induced no changes in EPS8 distribution (Figure 4, A and C; Supplemental Table S1). Tubocurarine block for 1 DIV similarly reduced BAIAP2L2 at row 2 tips (Supplemental Figure S3A).

Past P4.5, hair-bundle morphology is not affected by tubocurarine (Krey *et al.*, 2020). We tested if BAIAP2L2 remained susceptible

filopodial tip signal per cell. Statistical significance was assessed by Kruskal–Wallis tests, followed by Dunn's multiple comparisons; *P* values are indicated in the plot (Supplemental Table S1 for details). (G) Constructs used for nanoscale pull down. (H) BAIAP2L2, EPS8, and MYO15A constructs used for pull-down experiments. BAIAP2L2 C-terminal domain carries the N-terminal GST tag. EPS8 and truncates carry N-terminal 6xHis-2xHA tags. MYO15A(tail) carries the N-terminal GFP tag. (I) Representative immunoblots of EPS8 and MYO15A(tail) pull down by BAIAP2L2 CT. EPS8 and truncates detected by anti-6xHis; MYO15A(tail) detected by anti-GFP. (J) Representative immunoblot of EPS8 and truncate pull down by BAIAP2L2-CT. Input lanes loaded with 2% (I), 0.4% (I, anti-GFP), or 1% (J, anti-6xHis) of total; 10% (I) or 25% (J) of total pull-down fractions (GST x, BAIAP2L2-CT x) were analyzed. Predicted MW of recombinant proteins (right); MW ladder sizes (left). (K) Previously reported interactions between MYO15A and EPS8 (black), as well as the BAIAP2L2-EPS8 interaction described here (red).

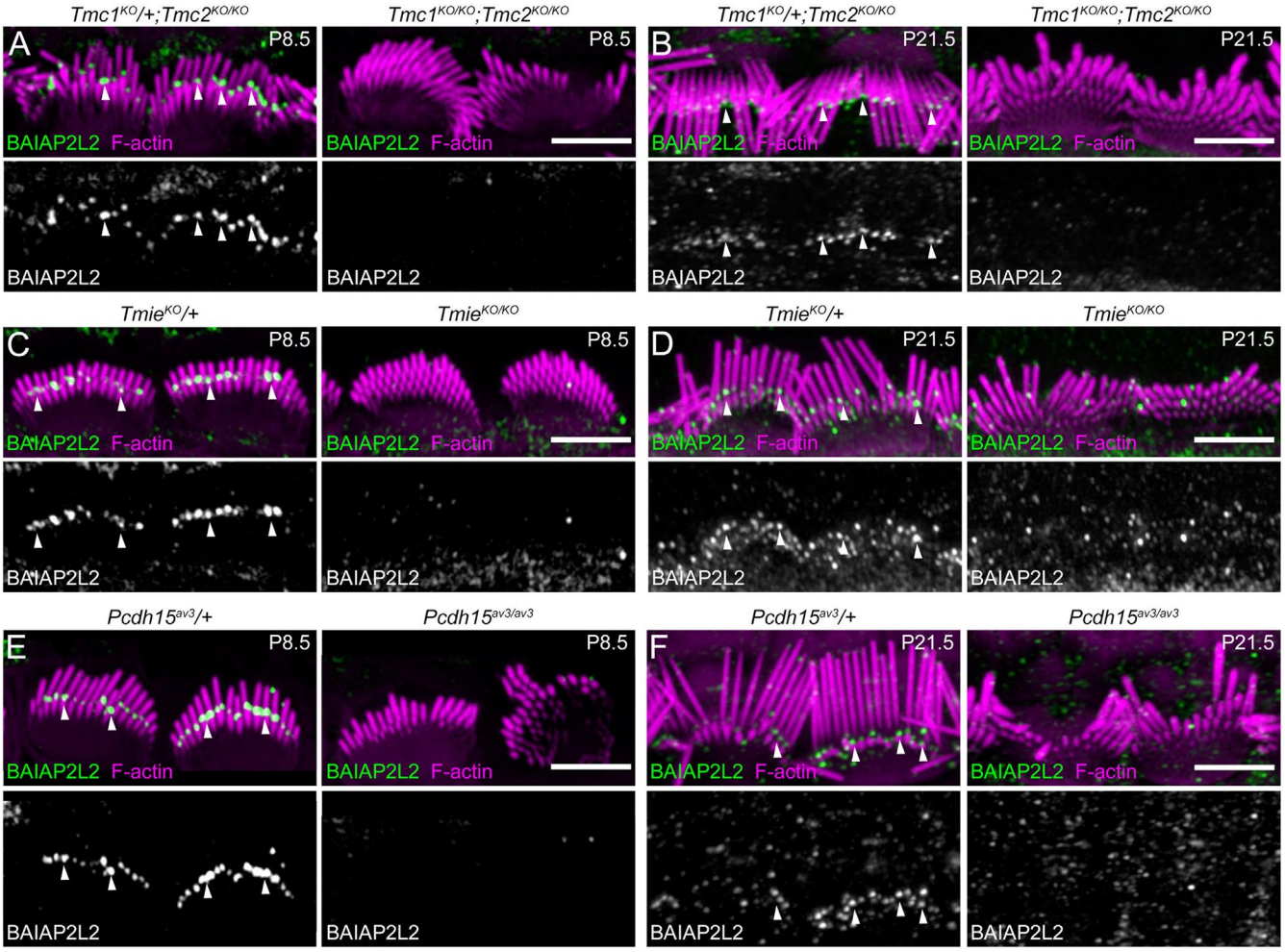

FIGURE 3: BAIAP2L2 is absent from stereocilia tips in transduction mutants. Anti-BAIAP2L2 signal in transduction mutant heterozygote and knockout IHCs at P8.5 (A, C, E) and P21.5 (B, D, F). In most images, hair bundles were flattened back toward the bare zone. Antibody signal intensity is matched between heterozygote and knockout pairs in each panel, but not comparable across ages or mutants. (A, B) *Tmc1*^{KO}/+; *Tmc2*$^{KO/KO}$ and *Tmc1*$^{KO/KO}$; *Tmc2*$^{KO/KO}$. In P21.5 heterozygote, the bundle is folded forward over the shorter stereocilia. (C, D) *Tmie*^{KO}/+ and *Tmie*$^{KO/KO}$. (E, F) *Pcdh15*^{av3}/+ and *Pcdh15*$^{av3/av3}$. Solid arrowheads at row 2 tips. Scale, 5 µm.

to transduction block in explants from C57BL/6J mice after the morphology critical period. When block was initiated at P8.5, tubocurarine treatment for 2 DIV still abolished BAIAP2L2 signal from bundles (Figure 4, D and E; Supplemental Table S1); as in P4.5+2 DIV bundles, tubocurarine treatment did not alter EPS8 distribution (Figure 4F; Supplemental Table S1).

We next asked whether the loss of BAIAP2L2 from tips could be reversed by relieving transduction block. Cochleas from P4.5 C57BL/6J mice were cultured in control media or in media with tubocurarine. At 2 DIV, media for all samples was replaced with control media, and explants cultured for 1 additional DIV (Figure 4G). BAIAP2L2 and EPS8 were immunolocalized at 2 DIV (prewashout) and at 3 DIV (1 DIV postwashout) (Figure 4H). As before, BAIAP2L2 signal was abolished after 2 DIV with tubocurarine (Figure 4I; Supplemental Table S1). At 1 DIV postwashout, BAIAP2L2 signal returned to row 2 tips (Figure 4I; Supplemental Table S1). EPS8 row 1 signal remained higher than row 2 signal, regardless of treatment.

These experiments indicated that the association of BAIAP2L2 with stereocilia tips relies on the continuous action of active transduction channels. An acute block of transduction led to the loss of BAIAP2L2 even after it had targeted to stereocilia tips, suggesting that BAIAP2L2's maintenance there required open channels. Full restoration of BAIAP2L2 to stereocilia tips after relieving transduction block further reinforced the suggestion that continuous transduction was required for targeting and raised the possibility that BAIAP2L2's retention at transducing stereocilia may require active transduction throughout the lifetime of the hair bundle. By contrast, localization of EPS8 at the tips of row 1 was largely insensitive to transduction block.

Ca^{2+} retains BAIAP2L2 at stereocilia tips

We hypothesized that BAIAP2L2's retention at stereocilia tips relies on Ca^{2+}-mediated membrane association. To test this model, we expressed BAIAP2L2(I-BAR)-mCherry in HeLa cells (Figure 5B) and subjected the transfected cells to treatment with 2 µM ionomycin (iono), a Ca^{2+} ionophore (Liu and Hermann, 1978). We supplemented solutions with either 5 mM EGTA or 20 µM $CaCl_2$ to lower or raise the intracellular Ca^{2+} concentration near the plasma membrane. As a control, cells were also subjected to either 5 mM EGTA or 20 µM $CaCl_2$ with the carrier DMSO in place of iono. As an additional control, we expressed the $PI(4,5)P_2$ sensor PLCD1(PH)-GFP

(Varnai and Balla, 1998) in HeLa cells (Figure 5A) and subjected the transfected cells to the conditions outlined above.

In the PLCD1(PH)-transfected cells, PH membrane association was evident under all conditions tested (Figure 5A). However, treatment with iono and $CaCl_2$ together increased the level of cytoplasmic PH and resulted in a significantly lower level of PH membrane enrichment than did treatment with DMSO and $CaCl_2$ together (Figure 5C; Supplemental Table S1). As elevated Ca^{2+} has been shown to inhibit $PI(4,5)P_2$ recognition by PLCD1(PH) (Bilkova *et al.*, 2017), the observed decrease in relative membrane association for iono and $CaCl_2$ together was expected.

In BAIAP2L2(I-BAR)-transfected cells, treatment with iono and $CaCl_2$ together significantly elevated I-BAR membrane enrichment over the other conditions (Figure 5D; Supplemental Table S1). The I-BAR domain of BAIAP2L2 thus was attracted to plasma membranes when local Ca^{2+} levels were elevated.

To test if BAIAP2L2 localization in hair bundles also displayed Ca^{2+} dependence, we cultured cochlear explants from C57BL/6J mice for 2 DIV in the presence or absence of 20 µM BAPTA-AM, a cell-permeant Ca^{2+} chelator. As before, EPS8 and BAIAP2L2 were immunolocalized after the 2 DIV and their tip signal quantified (Figure 5, G–I). We found that reduction of intracellular Ca^{2+} with BAPTA-AM, like acute channel block, strongly attenuated BAIAP2L2 signal at row 2 tips (Figure 5H; Supplemental Table S1). Abolition of row 2 BAIAP2L2 tip signal was less complete with BAPTA-AM than with tubocurarine, however, and row 1 BAIAP2L2 tip signal was unexpectedly significantly elevated with BAPTA-AM (Figure 5H; Supplemental Table S1). BAIAP2L2 was still largely retained at row 2 tips after treatment with BAPTA-AM for 1 DIV (Supplemental Figure S3B). The EPS8 signal, however, showed no response to the BAPTA-AM treatment (Figure 5I; Supplemental Table S1). Buffering intracellular Ca^{2+} thus recapitulated the effect of blocking transduction in cochlear explants; when Ca^{2+} was reduced, less BAIAP2L2 was present at row 2 stereocilia tips.

Divalent cations such as Ca^{2+} can induce clustering of phosphoinositides, specifically $PI(4,5)P_2$ (Ellenbroek *et al.*, 2011; Bradley *et al.*, 2020), and lipid recognition by proteins can be modulated by changes in lipid conformation (Bilkova *et al.*, 2017). BAIAP2L2 has no identified Ca^{2+}-binding sites but does display a broad preference toward phosphoinositide-containing membranes (Pykalainen *et al.*, 2011); the I-BAR domain of BAIAP2L2 may therefore bind clusters of Ca^{2+}-bound phosphoinositides. Alternatively, BAIAP2L2 might be localized at stereocilia tips by CIB2, a Ca^{2+}-sensitive component of the transduction complex (Liang *et al.*, 2021). CIB2 interacts with BAIAP2L2 (Yan *et al.*, 2021); if CIB2 tethers BAIAP2L2 to stereocilia tips, the BAIAP2L2-CIB2 interaction might require Ca^{2+}-bound CIB2.

CONCLUSIONS

BAIAP2L2 delivery to tips relies on the MYO15A-EPS8 complex, which is also involved in the targeting of several key proteins in stereocilia (Belyantseva *et al.*, 2005; Manor *et al.*, 2011; Tadenev *et al.*, 2019). MYO15A-2 and EPS8 do not accumulate to high levels at row 2 tips, so once BAIAP2L2 reaches its target, the motor complex may shuttle back to the hair cell's cytoplasm. In *Eps8*-null stereocilia, which have significant transduction currents (Zampini *et al.*, 2011), BAIAP2L2 may depend on a different MYO15A complex to transport it to tips.

BAIAP2L2 is at stereocilia tips only when transduction channels are present and open, which explains why BAIAP2L2 is enriched in transducing stereocilia and not in row 1. In wild-type hair cells, potent buffering of Ca^{2+} (Hackney *et al.*, 2005) and transport by Ca^{2+} pumps (Yamoah *et al.*, 1998) limits Ca^{2+} diffusion and should ensure that the membrane-bound BAIAP2L2 remains close to transduction channels. Higher levels of BAIAP2L2 at tips of row 2 versus row 3 may result either from hypothesized elevated Ca^{2+} entry (Krey *et al.*, 2020) or from the flatter membrane at row 2 tips, favored for BAIAP2L2 (Krey *et al.*, 2020). I-BAR proteins like BAIAP2L2 also deform membranes (Mattila *et al.*, 2007; Pykalainen *et al.*, 2011), which suggests that BAIAP2L2 could influence the physical state of the stereocilia tip membrane.

Finally, elevated Ca^{2+} enhances association of BAIAP2L2's I-BAR domain with plasma membrane, consistent with the observation that chelation of intracellular Ca^{2+} leads to loss of BAIAP2L2 from stereocilia tips. Although the mechanism by which Ca^{2+} enhances membrane binding of BAIAP2L2 is not known, the slow loss of BAIAP2L2 after transduction block suggests that Ca^{2+} induces a relatively stable membrane interaction that is not immediately reversed after reduction of Ca^{2+} levels.

In summary, BAIAP2L2 is transported by the MYO15A-EPS8 complex in stereocilia and is retained selectively at the tips of transducing stereocilia because continuous Ca^{2+} influx through open transduction channels produces an environment that favors association of BAIAP2L2 with the plasma membrane (Figure 5J). Ca^{2+} is thus the transduction-specific factor responsible for retaining BAIAP2L2 at stereocilia tips, and its entry via channels provides the signal to modulate the protein environment at stereocilia tips.

MATERIALS AND METHODS

Request a protocol through *Bio-protocol*.

Animal lines

All animal procedures were approved by the Institutional Animal Care and Use Committee (IACUC) at Oregon Health & Science University (protocol IP00000714). Mouse pups were assumed to be born at midnight, so the animal age on the first day is referred to as P0.5. Both female and male pups were used for all experiments.

C57BL/6J mice (RRID:IMSR_JAX:000664, Jackson Laboratories, Bar Harbor, ME) were used for localization, proximity ligation, and explant culture assays. BAIAP2L2 localization was assessed in *Myo15a*^{sh2} (RRID:IMSR_JAX:000109, Jackson Laboratories) (Probst *et al.*, 1998) and *Myo15a*$^{\Delta N}$ (Fang *et al.*, 2015) lines, which have been previously described, as well as in *Eps8*$^{\Delta 818}$, which was newly generated via i-GONAD (Ohtsuka and Sato, 2019). *Myo15a*$^{\Delta N}$ tissue was a kind gift from Jonathan Bird. BAIAP2L2 localization was also assessed in *Tmc1*^{KO} and *Tmc2*^{KO} double knockout (Kawashima *et al.*, 2015), *Tmie*^{KO} (Zhao *et al.*, 2014), and *Pcdh15*^{av3} (Pawlowski *et al.*, 2006) lines. Animals have been maintained on a C57BL/6J background. *Myo15a*$^{\Delta N}$, *Tmc* double KO, *Tmie*^{KO}, and *Pcdh15*^{av3} mice were genotyped using previously described primers (Pawlowski *et al.*, 2006; Zhao *et al.*, 2014; Fang *et al.*, 2015; Kawashima *et al.*, 2015). Genotyping of *Myo15a*^{sh2} mice was performed by TransnetYX, Inc. (Cordova, TN). *Eps8*$^{\Delta 818}$ mice were genotyped using the following primers: wild-type forward primer (exon 3), 5′-AAG GCT CTG GCT TTC CTC TG-3′; wild-type reverse primer (exon 3), 5′-TGA TTG AAA CAT CAT CCC TTG GG-3′; and wild-type reverse primer (exon 5), 5′-CAG GGG TCG TTG TGA TTC CA-3′; the sequence targeted by wild-type reverse primer (exon 3) is lacking in *Eps8*$^{\Delta 818}$ mice. Phenotypes in all mutants were obvious so blinding to genotype was impossible.

Generation of Eps8$^{\Delta 818}$

The *Eps8* locus was targeted for CRISPR-mediated knockout using guide RNAs (gRNAs) designed to exons 3 and 5 (http://crispor.tefor.net/). gRNAs were delivered via in situ electroporation using the

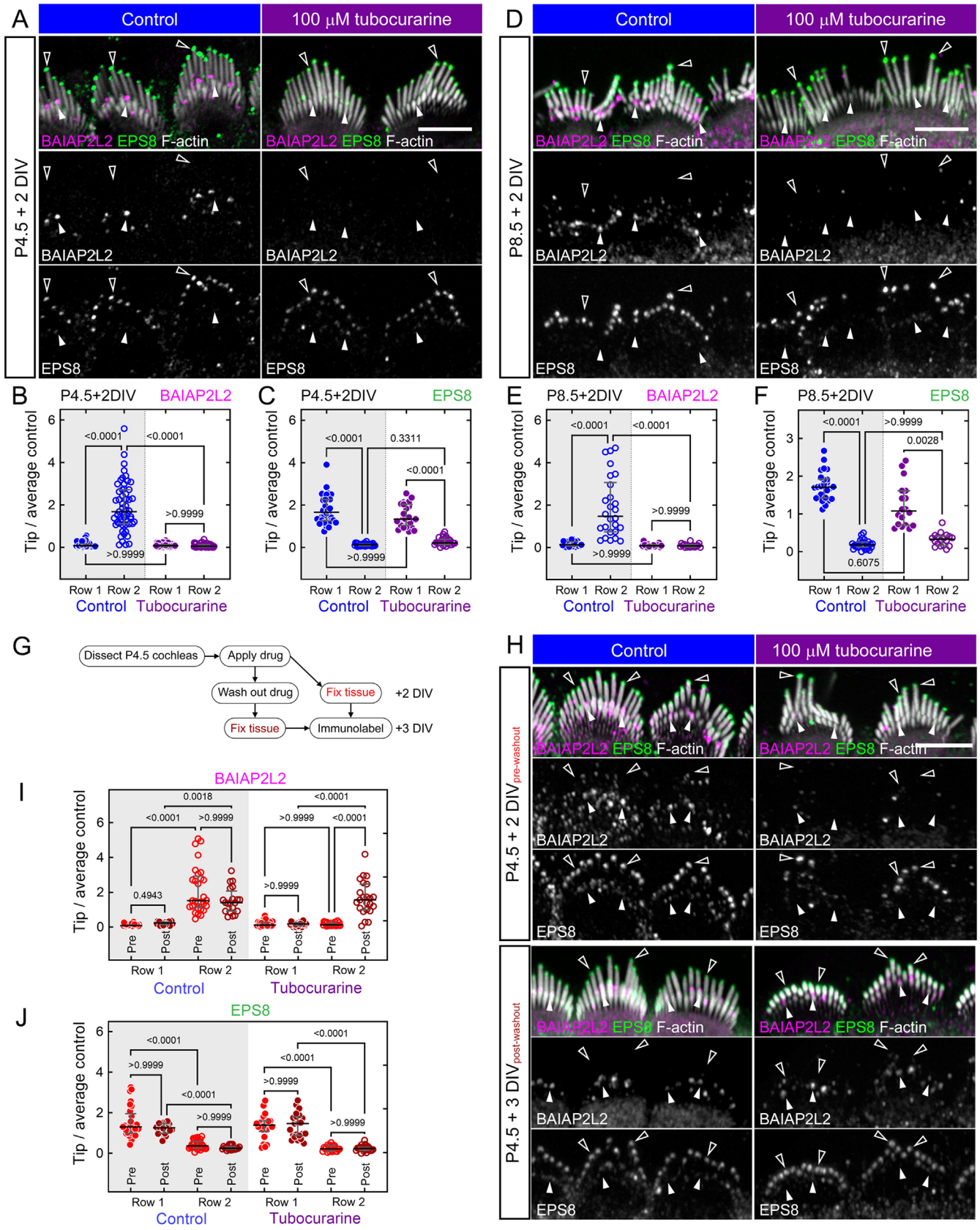

FIGURE 4: BAIAP2L2 tip enrichment is reversibly inhibited by transduction block. Anti-BAIAP2L2 and anti-EPS8 signal in IHCs of C57BL/6J cochleas cultured for 2 DIV with 100 μM tubocurarine. Cochleas were dissected at either P4.5 (A) or P8.5 (D). (B, C, E, F) Quantitation of BAIAP2L2 (C, E) and EPS8 (D, F) signal from A and B. Signal was normalized to average control signal of a given experiment. (G) Wash-in/out experiment design. (H) Anti-BAIAP2L2 and anti-EPS8

i-GONAD procedure (Gurumurthy *et al.*, 2019; Ohtsuka and Sato, 2019). Necessary components including guides (Alt-R CRISPR-Cas9 crRNA, exon 3 guide—ATATGTCTAACCGCTCCAGT, exon 5 guide—TCTTACTTCCACGCGGTACT), tracrRNA (Cat# 1072532), and Cas9 protein (Cat# 1081060) were obtained from Integrated DNA technologies (IDT). Timed crosses with two female and one male C57BL/6J mice were set for an E0.7 pregnancy. At this point in pregnancy, the zygote is at the single-cell stage and has lost its cumulus cells, allowing higher efficiency electroporation of the zygotes (Gurumurthy *et al.*, 2019). Pregnancy was confirmed by checking plugs. Ribonucleoprotein (RNP) was prepared. To anneal tracrRNA and crRNA, tracrRNA and crRNA were mixed to a final concentration of 60 and 30 µM, respectively, in Duplex buffer (IDT Cat# 1072570), then heated to 95˚C and allowed to cool slowly back to room temperature. Cas9 protein was added at a final concentration of 1.5 µg/ml to the annealed tracrRNA/crRNA mix, and the sample was heated to 37˚C and allowed to cool slowly back to room temperature. Fast Green (Fisher Scientific Cat# 2353-45-9) was prepared in Duplex buffer and then sterile-filtered through a 0.22-µm filter (Millipore Cat# SLGP033RS). Filtered Fast Green was added at 3 mg/ml to the RNP sample so that the mixture could be visualized once injected within the oviduct. To prepare for electroporation of RNPs, pregnant dams (E0.7) were given an intraperitoneal injection of anesthetic (working stock: 9 mg/ml Nembutal, Sigma Cat# P37610; 20.8 mg/ml $MgSO_4$, Sigma Cat# 63138; 10% ethanol, Sigma Cat# 459836; 40% propylene glycol, Fisher Scientific Cat# P335-1) at 7.8 µl per gram body weight; anesthesia was confirmed by the lack of toe pinch reflex. Surgery was performed to expose the ovary and oviduct, and an estimated 0.5 to 1 µl of the RNP mixture was injected into the lumen of the oviductal ampulla. The paddles of the electrode were placed around the portion of the oviduct where the Fast Green was visible, and electroporation was performed using three pulses of 5 ms On and 50 ms Off at 30 V. The range of currents achieved under this protocol was from 100 to 500 mA; optimal surgeries were in the range of 150–250 mA. After electroporation, ovary and oviduct were gently returned to the abdominal cavity, and the incision closed with two stitches and a wound clip. Throughout the surgery, tissue was kept hydrated with prewarmed Lactated Ringers Solution (Baxter Cat# 2B2323). For the first 3 d after surgery, dams were treated with a dose of Meloxicam (MWI Animal Health Cat# 501080) at 1 µl per gram body weight for pain management; the first dose was administered soon after surgery was complete. G0 pups were screened for mutations by PCR and sequencing. Genomic DNA was extracted from G0 tissue samples; using primers set to amplify any sequence containing a deletion between the targeted exons, PCR was performed, and amplicons were gel-purified and then were sequenced. A founder containing a large deletion spanning 10,818 base pairs of genomic DNA between exons 3 and 5 was identified, backcrossed onto the C57BL/6 background, and propagated as the Δ818 line used in this study. This mouse line is available on reasonable request.

Cell lines

For nanoscale pull-down experiments and plasma membrane-association studies, HeLa cells were obtained directly from ATCC (ATCC, CCL-2; RRID:CVCL_0030). For protein production, HEK 293T/17 cells were obtained directly from ATCC (ATCC, CRL-11268; RRID:CVCL_1926). Cells were cultured at 37°C (5% CO_2) in EMEM (Fisher Scientific Cat# 30-2003) supplemented with 10% serum plus medium supplement (Sigma Aldrich Cat# 14008C), 100 U/ml penicillin-G, and 100 µg/ml streptomycin (Sigma-Aldrich Cat# P4333). All experiments in HeLa cells were conducted between passages 10 and 40; HEK293T/17 cells were used to produce protein at passage 9. Cultures were confirmed mycoplasma negative with the LookOut Mycoplasma PCR Detection Kit (Millipore Sigma Cat# MP0035).

Immunofluorescence localization

For immunofluorescence, inner ears were isolated from mice of the indicated ages and genotypes and dissected in cold Hank's balanced salt solution (Thermo Fisher Scientific Cat# 14025076) supplemented with 5 mM HEPES, pH 7.4. During inner ear dissection, small openings were made in the periotic bones to allow perfusion of the fixative. Ears were fixed in 4% formaldehyde (Electron Microscopy Sciences Cat# 1570) in 1× PBS for 25 min at room temperature and washed twice for 5 min each in 1× PBS; cochleas were then dissected from periotic bones and the lateral wall was removed. Cochleas were permeabilized in 0.2% Triton X-100 in 1× PBS for 10 min, blocked in 5% normal donkey serum (Jackson ImmunoResearch Cat# 017-000-121) diluted in 1× PBS (blocking buffer) for 1 h at room temperature, and then incubated overnight at 4°C with primary antibodies diluted in blocking buffer. Samples were washed two times in 1× PBS after incubation with primary antibodies. Dilutions were 1:200 for anti-BAIAP2L2 (Abcam Cat# ab224323), 1:150 for the Atlas anti-BAIAP2L2 (Sigma-Aldrich Cat# HPA003043, RRID:AB_2227864), and 1:250 for both anti-EPS8 (BD Transduction Laboratories Cat# 610143; RRID:AB_397544) and anti-pan-MYO15A (PB48, Thomas Friedman lab). The BAIAP2L2 antibodies were validated in this study and in our previous report (Carlton *et al.*, 2021), the EPS8 antibody was validated here, and the MYO15A antibody was validated previously (Belyantseva *et al.*, 2003). Cochleas were then incubated with secondary antibodies, which were either 2 mg/ml donkey anti-mouse Alexa Fluor 488 (Thermo Fisher Scientific Cat# A21202; RRID:AB_141607) or 2 mg/ml donkey anti-rabbit Alexa Fluor 568 (Thermo Fisher Scientific Cat# A10042; RRID:AB_2534017), for 3–4 h at room temperature; 1 U/ml CF488A phalloidin (Biotium Cat# 00042) was also included for single-antibody experiments during the incubation with secondary antibodies, while 1 U/ml CF405 phalloidin (Biotium Cat# 00034) was instead included for two-antibody experiments. Tissue was washed three times in 1× PBS and mounted on a glass slide in approximately 50 µl of Vectashield (Vector Laboratories Cat# H-1000) and covered with a #1.5 thickness 22 × 22 mm cover glass (Corning Cat# 2850-22). Cochlear hair bundles were imaged using a 63× 1.4 NA Plan-Apochromat objective on a Zeiss LSM980 system equipped with an

signal in IHCs of C57BL/6J cochleas dissected at P4.5 and cultured for 2 DIV with 100 µM tubocurarine, followed by washout of original media and 1 additional DIV after washout. (I, J) Quantitation of BAIAP2L2 (I) and EPS8 (J) signal from (H). Post-washout signal was normalized to control prewashout signal. Antibody signal intensity was matched between control and tubocurarine pairs for each experiment. Data are plotted with median and IQR; a point represents the average normalized tip signal for a single IHC. Statistical significance was assessed by Kruskal–Wallis tests, followed by Dunn's multiple comparisons; *P* values are indicated in the plots (Supplemental Table S1 for details). Empty arrowheads at row 1 tips, solid arrowheads at row 2 tips. Scale, 5 µm.

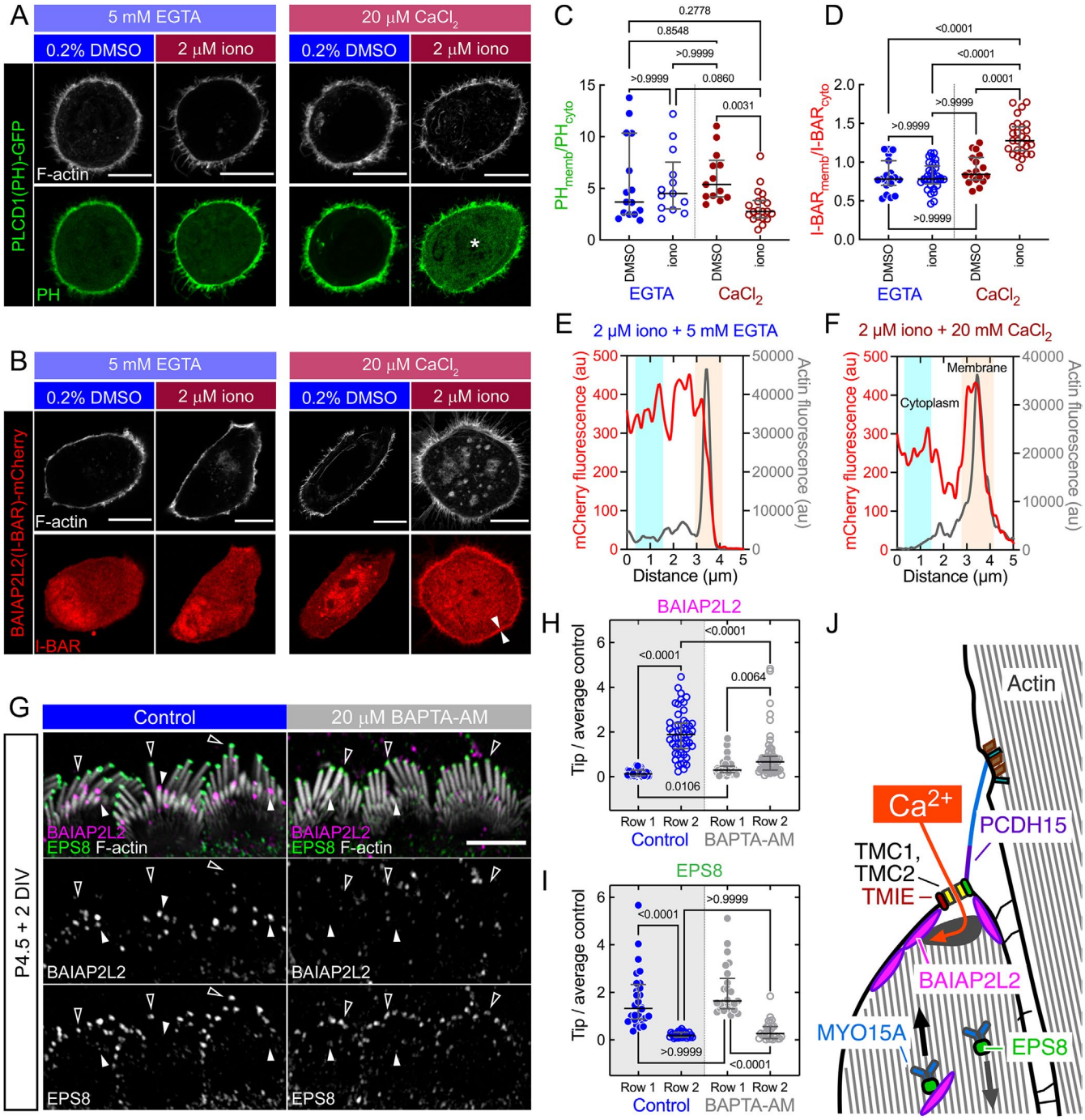

FIGURE 5: Ca^{2+} mediates row 2 tip enrichment of BAIAP2L2. (A, B) HeLa cells expressing PLCD1(PH) with a C-terminal GFP tag (A) or BAIAP2L2(I-BAR) with a C-terminal mCherry tag (B). Cells treated with 0.2% DMSO or 2 μM iono supplemented with 5 mM EGTA or 20 μM $CaCl_2$. Fluorescence intensity was adjusted per cell. In iono/Ca^{2+}-treated samples, the asterisk indicates elevated PLCD1(PH) in the cytoplasm and arrowheads indicate increased BAIAP2L2(I-BAR) at the membrane. (C, D) Quantitation of membrane enrichment for PLCD1(PH) (C) or BAIAP2L2(I-BAR) (D) under indicated conditions. (E, F) Example line scans of BAIAP2L2(I-BAR) and F-actin (phalloidin) signal from iono-treated cells with (E) EGTA or (F) $CaCl_2$. (G) Anti-BAIAP2L2 and anti-EPS8 signal in IHCs from P4.5 C57BL/6J cochleas cultured for 2 DIV with 20 μM BAPTA-AM. (H, I) Quantitation of BAIAP2L2 (H) and EPS8 (I) signal (as in Figure 4). (J) Summary schematic depicting BAIAP2L2 transport by MYO15A-EPS8 and Ca^{2+}-aided retention in stereocilia. Data are plotted with median and IQR. Statistical significance was assessed by Kruskal–Wallis tests, followed by Dunn's multiple comparisons; In B and D, a point is the average ratio of membrane/cytoplasm signal per cell. In H and I, a point is the average tip signal for a single IHC. *P* values are indicated in the plots (Supplemental Table S1 for details). Scale: A, 10 μm; E, 5 μm.

Airyscan2 detector and ZEN 3.3 (blue edition, 64-bit software; Zeiss, Oberköchen, Germany) acquisition software. Manufacturer-suggested settings for optimal Nyquist-based resolution were used for x-y pixel resolution, z-spacing, as well as pinhole diameter. Raw data processing for Airyscan-acquired images was performed using manufacturer-implemented automated settings. For each antibody, two to three images were acquired from one to three cochlea per genotype per age for each experiment, and experiments were conducted at least twice. Ears from control and mutant littermates were stained together and imaged together for each experiment to limit variability. During image acquisition, the gain and laser settings for the antibody and phalloidin signals were set to reveal the staining pattern in control samples, and the corresponding mutant samples used the same settings. Display adjustments in brightness and contrast were made using Fiji/ImageJ software, as were maximum, average, and/or sum Z-projections.

For PLAs, tissue processing and staining with primary antibodies were performed as outlined above. The anti-BAIAP2L2, anti-EPS8, and anti-pan-MYO15A antibodies were used at the same dilutions as above, and anti-RDX (Abnova Cat# H00005962-M06; RRID:AB_464027) was used at 1:100. After incubation with primary antibodies, proximity ligation was performed according to the manufacturer's specifications (Duolink In Situ PLA; Sigma Aldrich Cat#s DUO92004, DUO92002, DUO92008). Counterstaining with 1 U/ml CF488A phalloidin was performed as described above, and samples were imaged with the same considerations as detailed above.

Expression constructs

PCR amplification and cloning were performed using standard methods, and expression constructs were verified by Sanger sequencing. Plasmid DNA for transfection of mammalian cells was prepared using endotoxin-free purification kits (Plasmid Plus Midi Kit, Qiagen Cat# 12943). Plasmid DNA for transformation of BL21(DE3) *Escherichia coli* (New England Biolabs Cat# C2527) was prepared using smaller scale purification kits (ZR plasmid Miniprep Cat# Fisher Scientific, D4016).

For nanoscale pull down, the GFP-tagged MYO10 HMM [*Gfp-Myo10*(HMM)] construct (aa 1–946, NP_776819) was a kind gift from Richard Cheney; this construct encompasses the MYO10 ATPase motor and three tandem IQ motifs. A MYO15A(tail) construct (aa 1973–2943, NP_001096641) [*gfp-Myo15a*(tail)] was a kind gift from Jonathan Bird and includes two MyTH-FERM repeats and an SH3 domain. To create a bait construct for nanoscale pull down (Bird *et al.*, 2017), *Myo15a*(tail) was fused to *Myo10*(HMM) [*gfp-Myo10*(HMM)-*Myo15a*(tail)]. Two prey constructs were created, one expressing BAIAP2L2 N-terminally tagged with mCherry (*mCherry-Baiap2l2*) and the other expressing EPS8 N-terminally tagged with myc (myc-*Eps8*) and mCherry-BAIAP2L2 separated by a self-cleaving P2A peptide (*myc-Eps8/P2A/mCherry-Baiap2l2*). Construct schematics are shown in Figure 2G.

For in vitro pull down, the GST-tagged BAIAP2L2 C-terminal domain and 6xHis-2xHA-tagged EPS8 constructs were the same used previously (Carlton *et al.*, 2021). Deletion truncates of EPS8 were generated from the original 6xHis-2xHA-tagged EPS8 construct using a commercial mutagenesis kit (Q5 Site-Directed Mutagenesis Kit; New England Biolabs Cat# E0554S). GST alone was expressed from an empty pGEX-4T3 vector (Cytiva, Cat# GE28-9545-52). GFP-MYO15A(tail) was expressed from the plasmid provided by Jonathan Bird. Construct schematics are shown in Figure 2H.

For plasma membrane-association studies, the I-BAR domain of BAIAP2L2 (aa 1–261, NP_808248) was cloned into a pRP[Exp]-CMV backbone with a C-terminal mCherry tag [*Baiap2l2*(I-BAR)-*mCherry*]. *Plcd1*(PH)-*gfp* was a gift from Tamas Balla (PH-PLCD1-GFP, Addgene plasmid # 51407, http://n2t.net/addgene:51407, RRID:Addgene_51407).

Nanoscale pull down

HeLa cells were double-transfected using Lipofectamine 3000 (Thermo Fisher, L3000015) as detailed. Plasmid pairs were as follows: 1) *Gfp-Myo10*(HMM) + *mCherry-Baiap2l2*, 2) *Gfp-Myo10*(HMM)-*Myo15a*(tail) + *mCherry-Baiap2l2*, 3) *Gfp-Myo10*(HMM) + *myc-Eps8/P2A/mCherry-Baiap2l2*, and 4) *Gfp-Myo10*(HMM)-*Myo15a*(tail) + *myc-Eps8/P2A/mCherry-Baiap2l2*. Cells were incubated at 37°C for approximately 24 h posttransfection before being trypsinized and reseeded onto #1.5 thickness glass coverslips coated in 0.025 mg/ml poly-L-lysine (Sigma Aldrich, P1274). Reseeded cells were further incubated at 37°C for another 24 h and then washed once in 1× PBS, and fixed for 15 min in 4% formaldehyde at room temperature. Fixed cells were washed three times in 1× PBS before permeabilizing in 0.1% Triton-X100 in 1× PBS for 10 min and then incubated with 1 U/ml CF405 phalloidin in 1× PBS for 2–3 h at room temperature. Cells were washed three times in 1× PBS, and coverslips were mounted in Everbrite mounting medium (Biotium Cat# 23005). Imaging was performed on the same setup described above. Cells were imaged such that the field of view contained one to two cells with clearly extended filopodia that did not contact other cells, and so the z-stack encompassed the filopodia (i.e., the entire cell body was not imaged).

In vitro pull down with recombinant proteins

Pull-down assays were performed as described previously (Carlton *et al.*, 2021). Briefly, expression of GST alone, GST-tagged BAIAP2L2 C-terminal domain (CT, residues 262-522), and 6xHis-2xHA-tagged EPS8 constructs (residues 1–821 [full-length protein], 1–520, 208–520, 310–520, and 521–821) were induced in BL21(DE3) competent *E. coli* by the addition of 0.5 mM isopropyl β-D-1-thiogalactopyranoside (Sigma-Aldrich Cat# I-6758) and allowed to continue overnight at 25°C. To produce GFP-MYO15A(tail) protein, HEK293T/17 cells were transfected with *gfp-Myo15a*(tail) using Lipofectamine 3000 and allowed to express for 24 h. Cell extracts were prepared by sonication of cells resuspended in 1× PBS supplemented with a protease inhibitor cocktail (Sigma-Aldrich, P8465) and 0.5% Triton X-100. Sonicates were clarified by centrifugation at 12,000 × *g* for 30 min, and the supernatants (clarified extracts) were assessed for expression levels by immunoblotting prior to use in pull-down assays. Glutathione Sepharose 4B beads (Millipore Sigma Cat# 17-0756-01) were incubated with clarified bacterial extracts for 1 h at room temperature to load GST or GST-tagged BAIAP2L2 CT. GST-loaded beads were then washed in PBS for 3 × 5 min at 500 × *g*. To test if a tripartite complex between MYO15A, EPS8, and BAIAP2L2 could be formed (Figure 2I), the GST-loaded beads were then incubated with MYO15A-containing lysate in the absence or presence of EPS8. To map the EPS8-BAIAP2L2 interaction (Figure 2J), the GST-loaded beads were then incubated for 1 h at room temperature with EPS8-containing extracts to allow EPS8 binding of GST-tagged bait protein. Unbound proteins were removed by washing in PBS for 3 × 5 min at 500 × *g*. Beads were transferred to spin columns, incubated for 10 min with hot 2× LDS sample buffer (Invitrogen Cat# NP0007) and then spun for 5 min at 1000 × *g* to elute complexes into 2× reducing agent (Invitrogen, NP0009). Pull-down samples and input lysates were analyzed by immunoblotting and detected with rabbit anti-GST (Santa Cruz Cat# sc-33613; RRID:AB_647588), mouse anti-6xHis (Proteintech Cat# 66005-1;

RRID:AB_11232599), or mouse anti-GFP (Santa Cruz Cat# sc-9996; RRID:AB_627695).

Cochlear explants

Explants were prepared essentially as described (Krey *et al*., 2020). Briefly, C57BL/6J mice were sacrificed at P4.5 or P8.5 using cervical dislocation, and the head was removed and the surface was sterilized by immersion in 70% ethanol for ~30 s. The heads were then allowed to air-dry for approximately 30 s, then they were bisected along the midsagittal plane and placed into DMEM/F12 containing L-glutamine and 15 mM HEPES (Sigma Aldrich Cat# D8062) supplemented with 10 mM sodium pyruvate (Thermo Fisher Scientific Cat#, 11360-070) and 30 µM penicillin G (Sigma-Aldrich Cat# P3032) (solution 1) for microdissection. The otic capsule was dissected out from the temporal bone and placed in a new dish with solution 1 before removing the cartilaginous capsule surrounding the cochlea and the stria vascularis. A stainless steel minutien pin (0.02 mm tip diameter, 0.2 mm rod diameter, 10 mm length; Fine Science Tools Cat# 26002-20,) was placed through the modiolus. The minutien pin was then secured to a custom sterile plastic tissue chamber (5–6 mm depth and 9 mm diameter; 200 µl vol) and was transferred to a well in a 24-well plate containing 1 ml of solution 1. Solution 1 was replaced 2× with DMEM/F12 supplemented with 10 mM sodium pyruvate, 30 µM penicillin G, and the same growth factors at the same concentrations used previously (solution 2). Solution 2 had either the presence or the absence of a drug (either 100 µM tubocurarine [Sigma Aldrich Cat# T2379] or 20 µM BAPTA-AM [Cayman Chemical Cat# 15551]). The two cochleas from the same animal were given different treatments (control or drug). Tissues were then incubated at 37°C (5% CO_2) for approximately 48 h and then fixed in 4% formaldehyde solution for 25 min at room temperature. For the washin/washout experiment shown in Figure 4, G–J, explants were not fixed after 48 h in vitro; instead, the culture solution was removed, exchanged three times with fresh solution 2 without tubocurarine, and then incubated for one additional day in vitro at 37°C (5% CO_2) before fixation in 4% formaldehyde solution for 25 min at room temperature. Fixed explants were washed twice for 5 min each in 1× PBS and then removed from their minutien pins to complete the microdissection of the organ of Corti. Explants were stained against BAIAP2L2 and EPS8 using the immunofluorescence and Airyscan imaging protocols described above; images were exclusively collected from the middle turn of the cochlea, as this region of tissue was disturbed the least during the process of placing cochleas into culture.

Plasma membrane-association studies

HeLa cells seeded on #1.5 thickness glass coverslips coated in 0.025 mg/ml poly-L-lysine were transfected with either *Plcd1*(PH)-*gfp* (Addgene Cat# 51407) or *Baiap2l2*(I-BAR)-*mCherry* again using Lipofectamine 3000 and then incubated at 37°C (5% CO_2) for approximately 24 h. After the 24-h incubation, cells were treated with 1) 0.2% DMSO (Sigma Aldrich Cat# D8418) + 5 mM EGTA (Sigma Aldrich Cat# E4378), 2) 2 µM iono (Sigma Aldrich Cat#, I3909) + 5 mM EGTA, 3) 0.2% DMSO + 20 µM $CaCl_2$ (Fisher Chemical Cat# C79), and 4) 2 µM iono + 20 µM $CaCl_2$ for 30 min at 37°C (5% CO_2). As iono selectively transports Ca^{2+} into the cytosol (Liu and Hermann, 1978), these conditions allowed the comparison of the effect on I-BAR or PH membrane association produced by raising or lowering the local Ca^{2+} concentration near the plasma membrane. After treatment, cells were processed as described above for nanoscale pull-down experiments and imaged on the same setup. Fields of view were selected to include one to two cells, z-stacks were set to encompass the majority of the cell body, and three to six cells were imaged per condition. Each treatment condition was repeated three times.

Quantification and data analysis

All data based on fluorescence intensity were collected in ImageJ (http://rsbweb.nih.gov/ij/) and analyzed in Excel (Microsoft) and Prism (Graphpad). Prism was used to prepare all plots and to perform any statistical analyses. To determine the appropriate statistical test, the normality of all data was assessed by applying the Shapiro–Wilk test in Prism. For all experiments, data from at least one of the conditions failed normality; accordingly, the nonparametric Kruskal–Wallis test with Dunn's multiple comparisons was used to evaluate differences among groups.

Nanoscale pull-down results were assessed largely as described (Bird *et al.*, 2017) (https://github.com/NanoSPD/NanoSPD/tree/master/macro). Sum projections of two to four slices of 0.15 µm thickness were used to fully span all filopodia. Using the sum projections, average line scans (line thickness = 20) along filopodia starting at the cell body and extending a few micrometers past the filopodia tip using the GFP and phalloidin signal as guides, were also prepared. The mCherry channel was turned off during tracing to avoid selection bias. Only filopodia >2 µm away from the cell body were analyzed, and a maximum of 10 filopodia were sampled per cell. GFP and mCherry line scan values were exported from ImageJ into an Excel file. In the Excel file, all line scan values were normalized by dividing the value at each position by the average signal across the entire scan to control for differing expression levels of GFP bait protein and mCherry-BAIAP2L2 from cell to cell. The maximum of the normalized GFP signal was used to determine the position of the filopodia tip. To capture the entire filopodia tip, index matching was used to retrieve the normalized mCherry signal for all positions ± 0.16 µm about the maximum GFP signal. The retrieved values were summed and the result considered the mCherry tip signal for a given filopodium. Tip signal was averaged for each cell.

Stereocilia tip signal intensity was assessed for signal obtained with PLA. Average projections of ~10–20 slices of 0.15 µm thickness encompassing the hair bundle from stereocilia tips to apical surface of the hair cell were created. The range in slice thickness used was due to variations in bundle orientation. Using a circular region of interest (ROI), PLA signal was measured at stereocilia tips. Six to eight stereocilia were measured from row 1 and row 2 per IHC, and the ROI area and mean gray value were recorded for each tip, as well as the number of slices used to generate the average projection. For each stereocilia tip ROI, a background ROI was also measured. Raw tip signal was computed as the ROI area multiplied by tip gray value minus background gray value and then multiplied by the number of slices used for the projection. For any tips where the calculation resulted in a negative number, the value was replaced with zero. Quantified PLA signal was then normalized in two separate ways. First, measured tip signal was normalized to the average of all tips measured for a cell to account for variability of the same PLA assay pair from experiment to experiment. Second, all PLA signals were normalized to the average of all MYO15A-EPS8 PLA signals, the most consistent of the antibody pairs, to compare the signal levels between different antibody pairs. Average row 1 and average row 2 signals for each cell were calculated from the normalized values from both methods.

Stereocilia tip signal intensity for anti-BAIAP2L2 and anti-EPS8 was assessed in cochlear explants, largely using the same method outlined above. To control for staining variability across experiments, average tip signal intensity was computed for all control tips in a given experiment (a set of explants dissected and placed into

culture on the same day) and averaged; all tip values within the given experiment were then divided by this average control value to normalize signals. Average row 1 and average row 2 signals for each cell were calculated from the normalized values.

Plasma membrane association of PLCD1(PH)-GFP or BAIAP2L2(I-BAR)-mCherry was assessed by comparison of signal intensity at the plasma membrane to signal intensity within the cytoplasm. Sum projections of three to six slices of 0.15 µm thickness were prepared to capture a middle section of the cell body such that the membrane closest to the coverslip was excluded. Using the sum projections, average line scans (line thickness = 10) were prepared; lines were drawn starting inside the cell body and extended a few micrometers past the cell border as demarcated by the phalloidin (F-actin) signal. The mCherry or GFP channel was turned off during tracing to avoid selection bias. Four scans were acquired for each cell. GFP/mCherry and phalloidin line scan values were exported from ImageJ into an Excel file. In the excel file, the peak of the phalloidin signal was interpreted as the cortical actin at cell border, and used as a proxy for the plasma membrane (Koster and Mayor, 2016). For each line scan, mCherry or GFP signal was summed over a 1-µm segment either at the phalloidin peak to capture the plasma membrane-associated signal (Figure 4, E and F; tan boxes) or within the cell body to capture the cytoplasmic signal (Figure 4, E and F; aqua boxes); membrane-associated signal was then divided by cytoplasmic signal to find the ratio of membrane-associated to cytoplasmic signal. Ratios were averaged for each cell analyzed. PLCD1(PH) and BAIAP2L2(I-BAR) results were analyzed separately.

Experimental replicates and n

PLA was performed three to five times for each antibody combination; each experiment used cochleas from 4–6 littermates; 19–62 IHCs were analyzed per condition (Figure 1, A–F).

Immunostaining experiments were conducted two to three times for each age and genotype; each experiment analyzed at least two animals per genotype from the same litter (Figure 1, G–L).

Transfections for nanoscale pull down were conducted three to five times; 12–22 cells were analyzed per condition (four to six cells analyzed per condition per experiment) (Figure 2, A–F).

Pull down by BAIAP2L2 C-terminal domain was conducted two to three times for each condition (Figure 2, I and J).

Immunostaining experiments were performed at least twice for each age and genotype; each experiment analyzed at least two animals per genotype from the same litter (Figure 3).

Forty-six to 55 IHCs were analyzed per condition pooled from three experiments with three to four littermate animals used per experiment (Figure 4B).

Twenty-seven to 32 IHCs were analyzed per condition pooled from two experiments with three to four littermate animals used per experiment (Figure 4C).

Eighteen to 26 IHCs were analyzed per condition pooled from two experiments with three to four littermate animals used per experiment (Figure 4, E and F).

Twenty to 29 IHCs were analyzed per condition pooled from two experiments with six to eight littermate animals used per experiment (Figure 4, I and J).

Thirteen to 20 cells were analyzed per condition pooled from three experiments (Figure 5, A and C).

Eighteen to 33 cells were analyzed per condition pooled from three experiments (Figure 5, B and D).

Fifty-one to 56 IHCs were analyzed per condition pooled from three experiments with three to four littermate animals used per experiment (Figure 5, G-I).

Comparisons and *n* used for each experimental condition are indicated in Supplemental Table S1.

ACKNOWLEDGMENTS

Jennifer Goldsmith provided excellent mouse husbandry. Jonathan Bird kindly provided us with *Myo15a*$^{\Delta N}$ tissue and the *egfp-Myo15a*(tail) plasmid; the *Gfp-Myo10*(HMM) plasmid was a gift from Richard Cheney. The pan-MYO15A antibody was generously provided by Tom Friedman. We thank Andy Griffith for the *Tmc1*^{KO} and *Tmc2*^{KO} mouse lines and Uli Müller for the *Tmie*^{KO} mouse line. Confocal microscopy was performed at the OHSU Advanced Light Microscopy Core at The Jungers Center (supported by P30 NS061800). The study was supported by a grant to P.G.B-G (National Institutes of Health, R01DC002368).

REFERENCES

Ahmed ZM, Goodyear R, Riazuddin S, Lagziel A, Legan PK, Behra M, Burgess SM, Lilley KS, Wilcox ER, Riazuddin S, *et al.* (2006). The tip-link antigen, a protein associated with the transduction complex of sensory hair cells, is protocadherin-15. J Neurosci 26, 7022–7034.

Belyantseva IA, Boger ET, Friedman TB (2003). Myosin XVa localizes to the tips of inner ear sensory cell stereocilia and is essential for staircase formation of the hair bundle. Proc Natl Acad Sci USA 100, 13958–13963.

Belyantseva IA, Boger ET, Naz S, Frolenkov GI, Sellers JR, Ahmed ZM, Griffith AJ, Friedman TB (2005). Myosin-XVa is required for tip localization of whirlin and differential elongation of hair-cell stereocilia. Nat Cell Biol 7, 148–156.

Beurg M, Fettiplace R, Nam JH, Ricci AJ (2009). Localization of inner hair cell mechanotransducer channels using high-speed calcium imaging. Nat Neurosci 12, 553–558.

Bilkova E, Pleskot R, Rissanen S, Sun S, Czogalla A, Cwiklik L, Rog T, Vattulainen I, Cremer PS, Jungwirth P, Coskun U (2017). Calcium directly regulates phosphatidylinositol 4,5-bisphosphate headgroup conformation and recognition. J Am Chem Soc 139, 4019–4024.

Bird JE, Barzik M, Drummond MC, Sutton DC, Goodman SM, Morozko EL, Cole SM, Boukhvalova AK, Skidmore J, Syam D, *et al.* (2017). Harnessing molecular motors for nanoscale pulldown in live cells. Mol Biol Cell 28, 463–475.

Bradley RP, Slochower DR, Janmey PA, Radhakrishnan R (2020). Divalent cations bind to phosphoinositides to induce ion and isomer specific propensities for nano-cluster initiation in bilayer membranes. R Soc Open Sci 7, 192208.

Carlton AJ, Halford J, Underhill A, Jeng JY, Avenarius MR, Gilbert ML, Ceriani F, Ebisine K, Brown SDM, Bowl MR, *et al.* (2021). Loss of Baiap2l2 destabilizes the transducing stereocilia of cochlear hair cells and leads to deafness. J Physiol 599, 1173–1198.

Cosgrove D, Zallocchi M (2014). Usher protein functions in hair cells and photoreceptors. Int J Biochem Cell Biol 46, 80–89.

Ebrahim S, Ingham NJ, Lewis MA, Rogers MJC, Cui R, Kachar B, Pass JC, Steel KP (2016). Alternative splice forms influence functions of whirlin in mechanosensory hair cell stereocilia. Cell Rep 15, 935–943.

Effertz T, Becker L, Peng AW, Ricci AJ (2017). Phosphoinositol-4,5-bisphosphate regulates auditory hair-cell mechanotransduction-channel pore properties and fast adaptation. J Neurosci 37, 11632–11646.

Ellenbroek WG, Wang YH, Christian DA, Discher DE, Janmey PA, Liu AJ (2011). Divalent cation-dependent formation of electrostatic PIP2 clusters in lipid monolayers. Biophys J 101, 2178–2184.

Fang Q, Indzhykulian AA, Mustapha M, Riordan GP, Dolan DF, Friedman TB, Belyantseva IA, Frolenkov GI, Camper SA, Bird JE (2015). The 133-kDa N-terminal domain enables myosin 15 to maintain mechanotransducing stereocilia and is essential for hearing. eLife 4, e08627.

Fettiplace R (2017). Hair cell transduction, tuning, and synaptic transmission in the mammalian cochlea. Compr Physiol 7, 1197–1227.

Fettiplace R, Kim KX (2014). The physiology of mechanoelectrical transduction channels in hearing. Physiol Rev 94, 951–986.

Glowatzki E, Ruppersberg JP, Zenner HP, Rusch A (1997). Mechanically and ATP-induced currents of mouse outer hair cells are independent and differentially blocked by d-tubocurarine. Neuropharmacology 36, 1269–1275.

Gurumurthy CB, Sato M, Nakamura A, Inui M, Kawano N, Islam MA, Ogiwara S, Takabayashi S, Matsuyama M, Nakagawa S, *et al.* (2019). Creation of CRISPR-based germline-genome-engineered mice

without ex vivo handling of zygotes by i-GONAD. Nat Protoc 14, 2452–2482.
Hackney CM, Mahendrasingam S, Penn A, Fettiplace R (2005). The concentrations of calcium buffering proteins in mammalian cochlear hair cells. J Neurosci 25, 7867–7875.
Hirono M, Denis CS, Richardson GP, Gillespie PG (2004). Hair cells require phosphatidylinositol 4,5-bisphosphate for mechanical transduction and adaptation. Neuron 44, 309–320.
Hudspeth AJ (1997). How hearing happens. Neuron 19, 947–950.
Kaltenbach JA, Falzarano PR, Simpson TH (1994). Postnatal development of the hamster cochlea. II. Growth and differentiation of stereocilia bundles. J Comp Neurol 350, 187–198.
Kawashima Y, Kurima K, Pan B, Griffith AJ, Holt JR (2015). Transmembrane channel-like (TMC) genes are required for auditory and vestibular mechanosensation. Pflugers Arch 467, 85–94.
Kitajiri S, Fukumoto K, Hata M, Sasaki H, Katsuno T, Nakagawa T, Ito J, Tsukita S, Tsukita S (2004). Radixin deficiency causes deafness associated with progressive degeneration of cochlear stereocilia. J Cell Biol 166, 559–570.
Koster DV, Mayor S (2016). Cortical actin and the plasma membrane: inextricably intertwined. Curr Opin Cell Biol 38, 81–89.
Krey JF, Chatterjee P, Dumont RA, O'Sullivan M, Choi D, Bird JE, Barr-Gillespie PG (2020). Mechanotransduction-dependent control of stereocilia dimensions and row identity in inner hair cells. Curr Biol 30, 442–454.e447.
Liang X, Qiu X, Dionne G, Cunningham CL, Pucak ML, Peng G, Kim YH, Lauer A, Shapiro L, Muller U (2021). CIB2 and CIB3 are auxiliary subunits of the mechanotransduction channel of hair cells. Neuron 109, 2131–2149.e2115.
Lin L, Shi Y, Wang M, Wang C, Lu Q, Zhu J, Zhang R (2021). Phase separation-mediated condensation of Whirlin-Myo15-Eps8 stereocilia tip complex. Cell Rep 34, 108770.
Liu C, Hermann TE (1978). Characterization of ionomycin as a calcium ionophore. J Biol Chem 253, 5892–5894.
Manor U, Disanza A, Grati M, Andrade L, Lin H, Di Fiore PP, Scita G, Kachar B (2011). Regulation of stereocilia length by myosin XVa and whirlin depends on the actin-regulatory protein Eps8. Curr Biol 21, 167–172.
Mattila PK, Pykalainen A, Saarikangas J, Paavilainen VO, Vihinen H, Jokitalo E, Lappalainen P (2007). Missing-in-metastasis and IRSp53 deform PI(4,5)P2-rich membranes by an inverse BAR domain-like mechanism. J Cell Biol 176, 953–964.
McGrath J, Tung CY, Liao X, Belyantseva IA, Roy P, Chakraborty O, Li J, Berbari NF, Faaborg-Andersen CC, Barzik M, *et al*. (2021). Actin at stereocilia tips is regulated by mechanotransduction and ADF/cofilin. Curr Biol 31, 1141–1153.e1147.
Menna E, Disanza A, Cagnoli C, Schenk U, Gelsomino G, Frittoli E, Hertzog M, Offenhauser N, Sawallisch C, Kreienkamp HJ, *et al*. (2009). Eps8 regulates axonal filopodia in hippocampal neurons in response to brain-derived neurotrophic factor (BDNF). PLoS Biol 7, e1000138.
Ohtsuka M, Sato M (2019). i-GONAD: A method for generating genome-edited animals without ex vivo handling of embryos. Dev Growth Differ 61, 306–315.
Pan B, Akyuz N, Liu XP, Asai Y, Nist-Lund C, Kurima K, Derfler BH, Gyorgy B, Limapichat W, Walujkar S, *et al*. (2018). TMC1 forms the pore of mechanosensory transduction channels in vertebrate inner ear hair cells. Neuron 99, 736–753.e736.
Pawlowski KS, Kikkawa YS, Wright CG, Alagramam KN (2006). Progression of inner ear pathology in Ames waltzer mice and the role of protocadherin 15 in hair cell development. J Assoc Res Otolaryngol 7, 83–94.
Postema MM, Grega-Larson NE, Neininger AC, Tyska MJ (2018). IRTKS (BAIAP2L1) elongates epithelial microvilli using eps8-dependent and independent mechanisms. Curr Biol 28, 2876–2888.e2874.
Probst FJ, Fridell RA, Raphael Y, Saunders TL, Wang A, Liang Y, Morell RJ, Touchman JW, Lyons RH, Noben-Trauth K, *et al*. (1998). Correction of deafness in shaker-2 mice by an unconventional myosin in a BAC transgene. Science 280, 1444–1447.
Pykalainen A, Boczkowska M, Zhao H, Saarikangas J, Rebowski G, Jansen M, Hakanen J, Koskela EV, Peranen J, Vihinen H, *et al*. (2011). Pinkbar is an epithelial-specific BAR domain protein that generates planar membrane structures. Nat Struct Mol Biol 18, 902–907.
Rehman AU, Bird JE, Faridi R, Shahzad M, Shah S, Lee K, Khan SN, Imtiaz A, Ahmed ZM, Riazuddin S, *et al*. (2016). Mutational spectrum of MYO15A and the molecular mechanisms of DFNB3 human deafness. Hum Mutat 37, 991–1003.
Soderberg O, Gullberg M, Jarvius M, Ridderstrale K, Leuchowius KJ, Jarvius J, Wester K, Hydbring P, Bahram F, Larsson LG, Landegren U (2006). Direct observation of individual endogenous protein complexes in situ by proximity ligation. Nat Methods 3, 995–1000.
Tadenev ALD, Akturk A, Devanney N, Mathur PD, Clark AM, Yang J, Tarchini B (2019). GPSM2-GNAI Specifies the tallest stereocilia and defines hair bundle row identity. Curr Biol 29, 921–934.e924.
Tilney LG, Derosier DJ, Mulroy MJ (1980). The organization of actin filaments in the stereocilia of cochlear hair cells. J Cell Biol 86, 244–259.
Varnai P, Balla T (1998). Visualization of phosphoinositides that bind pleckstrin homology domains: calcium- and agonist-induced dynamic changes and relationship to myo-[3H]inositol-labeled phosphoinositide pools. J Cell Biol 143, 501–510.
Velez-Ortega AC, Freeman MJ, Indzhykulian AA, Grossheim JM, Frolenkov GI (2017). Mechanotransduction current is essential for stability of the transducing stereocilia in mammalian auditory hair cells. eLife 6, e24661.
Yamoah EN, Lumpkin EA, Dumont RA, Smith PJ, Hudspeth AJ, Gillespie PG (1998). Plasma membrane Ca2+-ATPase extrudes Ca2+ from hair cell stereocilia. J Neurosci 18, 610–624.
Yan K, Zong W, Du H, Zhai X, Ren R, Liu S, Xiong W, Wang Y, Xu Z (2021). BAIAP2L2 is required for the maintenance of mechanotransducing stereocilia of cochlear hair cells. J Cell Physiol, http//doi.org/10.1002/jcp.30545.
Zampini V, Ruttiger L, Johnson SL, Franz C, Furness DN, Waldhaus J, Xiong H, Hackney CM, Holley MC, Offenhauser N, *et al*. (2011). Eps8 regulates hair bundle length and functional maturation of mammalian auditory hair cells. PLoS Biol 9, e1001048.
Zhao B, Wu Z, Grillet N, Yan L, Xiong W, Harkins-Perry S, Muller U (2014). TMIE is an essential component of the mechanotransduction machinery of cochlear hair cells. Neuron 84, 954–967.
Zhao H, Pykalainen A, Lappalainen P (2011). I-BAR domain proteins: linking actin and plasma membrane dynamics. Curr Opin Cell Biol 23, 14–21.